



Anhysteretic strains in ferroelectric ceramics under electromechanical loading

Chaimae Babori^{1,2,*} , Mahmoud Barati^{1,2,3}, Valentin Seguin^{1,2}, Romain Corcolle^{1,2} and Laurent Daniel^{1,2} 

¹ Université Paris-Saclay, CentraleSupélec, CNRS, Laboratoire de Génie Electrique et Electronique de Paris, 91192 Gif-sur-Yvette, France

² Sorbonne Université, CNRS, Laboratoire de Génie Electrique et Electronique de Paris, 75252 Paris, France

³ EMITECH Group, 3 Rue des Coudriers, 78180 Montigny-le-Bretonneux, France

E-mail: chaimae.babori@centralesupelec.fr

Received 22 March 2024, revised 20 June 2024

Accepted for publication 1 August 2024

Published 9 August 2024



Abstract

This study investigates anhysteretic strains in PZT ceramics. The anhysteretic curves are associated with a stable balanced state of polarization in the domain structure, excluding dissipative effects related to mechanisms such as domain wall pinning. Anhysteretic measurements are representative of an -ideal- scenario in which the material would undergo no energy loss due to dissipative processes, focusing on the stable and reversible aspects of the domain configuration. The different methodologies employed to measure deformations under electromechanical loading are presented, leading to the introduction of digital image correlation (DIC) as the chosen technique, recognized for its ability to capture detailed information on transverse and longitudinal strain. The article then describes a procedure developed to obtain anhysteretic strain and anhysteretic polarisation for different levels of compressive loadings. The subsequent presentation of the results of the transverse and longitudinal strain analyses provides valuable insights into the reversible and irreversible behavior of the material. They can be used as a basis for the thermodynamical modelling approaches grounded on separating reversible and irreversible contributions or as a validation of existing models describing anhysteretic behavior. The compressive stress affects both the shape of hysteretic and anhysteretic curves. The anhysteretic curve represents a stable equilibrium in the domain structure. Compressive stress reduces strain by affecting the pinning of domain walls. These points justify the interest in studying the effect of compressive stress on the anhysteretic behavior of ferroelectrics.

Keywords: ferroelectric materials, anhysteretic strain, reversible behavior, hysteresis, PZT, digital image correlation, piezoelectric coefficients

* Author to whom any correspondence should be addressed.



Original content from this work may be used under the terms of the [Creative Commons Attribution 4.0 licence](https://creativecommons.org/licenses/by/4.0/). Any further distribution of this work must maintain attribution to the author(s) and the title of the work, journal citation and DOI.

1. Introduction

Ferroelectric materials are widely used in actuators [1], sensors [2, 3], harvesting devices [4] and converters [5] due to their exceptional electro-mechanical properties. In the past decades, these properties have been extensively investigated by characterizing the hysteretic polarization and strain induced by an electrical loading or mechanical stress [6–10]. These studies have led to a better understanding of the impact of hysteretic effects on material properties, such as the electro-mechanical coupling coefficient d_{33} [11–13] and the dielectric permittivity ϵ_{33} [14]. They form an essential basis for making robust industrial designs [15], such as Ferroelectric Random Access Memory (FeRAM), where the polarisation-electric field hysteresis in ferroelectric materials is exploited for non-volatile memory storage [16]. Similarly, strain-electric field hysteresis has been deliberately utilized in the design of precision actuators and motors for applications requiring controlled mechanical movement [17].

The separation of reversible and irreversible contributions is crucial for understanding the behavior of ferroelectrics. Zhou *et al* in [18] estimated the reversible contribution of polarisation and strain by partially unloading the sample during the application of the electric field. While Rayleigh behavior has been associated by some authors with a so-called reversible contribution, despite dissipation occurring in the Rayleigh zone [19], the term ‘reversible’ is used here according to its fundamental meaning: the reversible part of the behavior is its non-dissipative component. Anhyseteric behavior then refers to the theoretical energy equilibrium a material would attain under an applied field if there were no hysteresis. Although it is practically impossible to eliminate hysteresis entirely, the method outlined in this paper and detailed in [20] approximates this behavior in a step-by-step manner. Anhyseteric curves offer another insight into the behavior of ferroelectric materials by showing their reversible contribution only as demonstrated in [20]. The non-reversible contribution can be deduced *a posteriori*, from the difference between hysteretic and anhyseteric responses.

Anhyseteric curves offer. Non-reversible processes are caused by internal defects such as lattice vacancies. These defects produce dissipative forces that impede the motion of domain walls. As a result, the material behavior is hysteretic, involving energy dissipation and the appearance of remanent polarisation and coercive field. Contrary to hysteretic curves, anhyseteric curves are independent of the dissipative phenomenon and only show the behavior of the material as it would be if these phenomena were inexistent. Such information can help the development of modelling tools to describe the behavior of ferroelectrics [21, 22].

In this paper, anhyseteric curves are obtained by the application of an exponentially decaying bipolar electric field [20]. The decaying electric field offers a way for domain walls to overcome defects and reach a true equilibrium state. This anhyseteric protocol was originally developed for ferromagnetic materials [23–26]. It was recently shown that it could be also successfully applied to ferroelectrics [20]. Anhyseteric

behavior has for instance been used for the study of temperature effect on reversible and non-reversible contributions in PZT [27]. In this paper a similar approach is applied for the first time to determine anhyseteric strains in ferroelectric materials. This last study gave a detailed explanation of the experimental procedure required to measure anhyseteric curves. It also showed a new way to separate the reversible and dissipative contributions to material properties. However, these studies were restricted to the measurement of the anhyseteric polarization only.

As for the hysteretic P - E loop, it is experimentally possible to measure the anhyseteric strain out of the classical S - E butterfly loop. Ferroelectric strain is classically measured by strain gauge [28] or linear variable displacement transducer (LVDT) [29]. These two methods require being positioned directly on the sample, and their suitability may be constrained, particularly when dealing with small samples. Moreover, they offer only one measurement point. These drawbacks are presently avoided by using the Digital Image Correlation (DIC) technique which is contactless and provides a bi-dimensional mapping of longitudinal and transverse strain on the sample [30].

The DIC technique was already introduced in a huge variety of studies, including smart materials such as shape memory alloys [31, 32] and magnetostrictive materials [33, 34]. Typically, the numerical displacement resolution of a DIC setup is about 10^{-2} px. The physical resolution depends on the image sampling length of the optical setup. Using a long distance microscope, it has been shown that ferroelectric strains could be monitored, as the displacement resolution becomes sub-micrometric [35]. The only requirement is that the surface of the sample contains optical trackers (namely, a speckle pattern) so that displacements can be extracted by the DIC program. The speckle can be natural [36, 37] or painted [35, 38].

In this work, an experimental protocol is proposed for measuring the longitudinal and transverse anhyseteric strains of a ferroelectric material under different levels of compressive stress using DIC. The classical P - E and S - E hysteretic loops are used as a reference for a quantitative comparison. The anhyseteric strain curves are used to extract the evolution of the apparent anhyseteric piezoelectric coefficients, the results show a difference between the evolution of the apparent anhyseteric and hysteretic piezoelectric coefficients. Beyond the method’s precision, the outcome can lay the groundwork for modelling approaches based on a separation between reversible and irreversible processes. Moreover, a deeper understanding of ferroelectric strain can provide valuable guidance for refining the performance of piezoelectric materials in various applications [38].

2. Experiment

2.1. Experimental setup

The test bench is specifically designed for the application of an uniaxial electromechanical loading along the direction 3, as illustrated in figure 1 [38], allowing the application of an

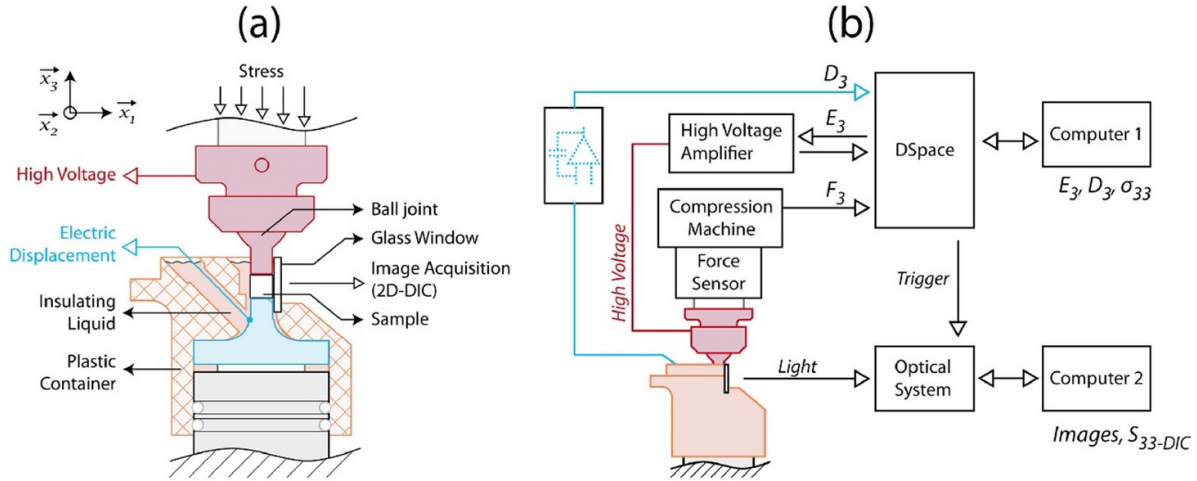


Figure 1. Illustration of the loading cell (a) and overview of the entire experimental setup (b) [38]. Reproduced from [38]. CC BY 4.0.

electric field up to 4 kV mm^{-1} and a compressive mechanical stress up to 100 MPa. The studied sample is a NCE55 from Noliac (commercial PZT). It is a $4 \times 4 \times 4 \text{ mm}$ sized bulk with silver electrodes and is initially unpoled. The specimen is positioned between two jaws, electrically insulated from the ground by alumina components and is immersed in a container filled with insulating liquid (Fluorinert FC-770) to prevent electric arcs. The upper jaw (highlighted in red) features a ball-joint mechanism connected to a High Voltage amplifier (TREK 20/20C-HS). The lower jaw (depicted in blue) is connected to a capacitor of $2057 \mu\text{F}$ [7, 8] to measure the electric displacement D_3 . All bearing surfaces have been precisely ground to ensure flatness within $\pm 4 \mu\text{m}$.

The compressive stress levels are ranged from 3 to 100 MPa. Throughout the experiment, the system maintains control of the applied stress, ensuring variations of no more than $\pm 6 \text{ MPa}$. The sample strain is measured by Digital Image Correlation (DIC). This technique allows the longitudinal and transverse strain components to be measured simultaneously. For this purpose, the sample is artificially speckled with white paint and a black powder according to [35]. The speckled face is one of the side faces, perpendicular to the electrodes. The sample is imaged during the tests using a 9.1 Mpx camera (Ximea MD091MU-SY) mounted on a microscope (Qeststar QM100). The image acquisition speed is set to its maximum value, i.e. 5 images per second. The captured images are post-processed by the program CorreliRT3 [39] to extract the strain values.

2.2. Experimental procedure

The anhysteretic polarization and strain curves are obtained in a discrete way, from a set of chosen electric field values E_{bias} . The anhysteretic curves are obtained from the collection of the response points $P_{\text{an}}(E_{\text{bias}})$ and $S_{\text{an}}(E_{\text{bias}})$, which are measured independently.

For illustration purpose, figures 2(a) and (b) show the applied electric field E as a function of time, for the two cases

$E_{\text{bias}} = 0$ and $E_{\text{bias}} = 2 \text{ kV mm}^{-1}$. Figures 2(c) and (d) show the corresponding polarisation response $P(t)$ of the sample.

The $E(t)$ signal consists in a sequence of four steps, as described in figure 2(a). Firstly, under a static compressive mechanical loading, the sample is subjected to an AC electric field with an amplitude E_A , so as to describe a major loop. In the 2nd step, an alternating decaying electric field [20] is imposed according to the following equation:

$$E(t) = E_A \sin(\omega t) \exp(-k\omega t) + E_{\text{bias}} [1 - \exp(-k\omega t)]. \quad (1)$$

With t the time, ω the angular frequency, E_A the electric field amplitude and E_{bias} the desired bias electric field. The remnant electric field amplitude targeted after N cycles is set as 2.23% of E_A . The parameters f , k , E_A and N were set according to the procedure described in [27]. The obtained values are $f = 0.5 \text{ Hz}$, $k = 0.015$, $E_A = 4 \text{ kV mm}^{-1}$ and $N = 69$. The desired bias electric fields for the anhysteretic curves are: $0, \pm 10, \pm 20, \pm 35, \pm 50, \pm 75, \pm 100, \pm 250, \pm 500, \pm 1000, \pm 1500, \pm 2000, \pm 3000 \text{ V mm}^{-1}$ for compressive stress of $-3, -25, -50, -75$ and -100 MPa .

After the N cycles, the 3rd step starts and the electric field is maintained constant, at E_{bias} . This step allows the anhysteretic points $P_{\text{an}}(E_{\text{bias}})$ and $S_{\text{an}}(E_{\text{bias}})$ to be measured (see figures 2(c) and 3). This measurement is however made from an unknown reference. A common and reliable reference must then be found between the different anhysteretic points. For this purpose, a sine electric field of amplitude E_A and frequency 50 mHz is added as a 4th step, to describe a major loop. The center of the P - E loop is used as a new polarization reference, by removing the quantity $(P_{\text{max}} + P_{\text{min}})/2$. It also helps in compensating the possible polarization drift [27] that may have occurred from steps one to three.

No strain information is measured during the first two steps (first major loop and decaying field). As described in the previous section, the anhysteretic strain is measured simultaneously by DIC. 10 images are obtained during the 3rd step and 100 during the last step. Every image acquired through digital image correlation provides a strain mapping across the entire

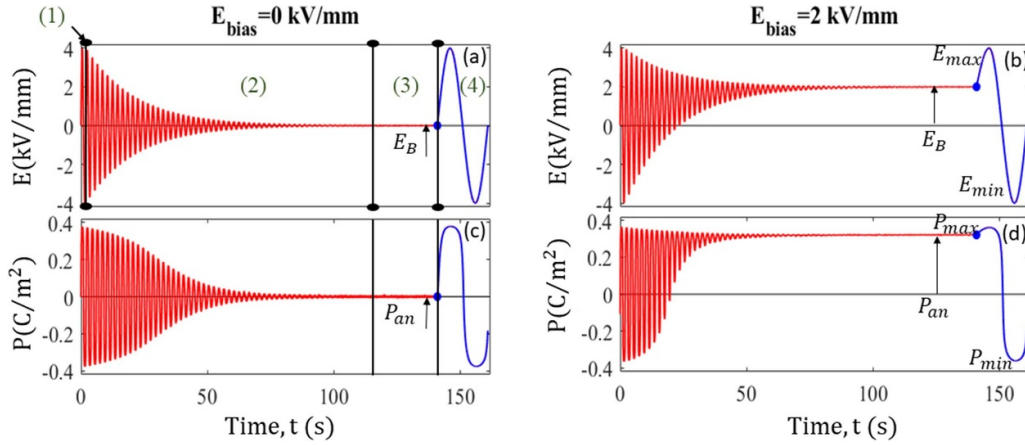


Figure 2. Electrical loading $E(t)$ used on NCE55 (PZT) to measure the anhyseretic point at bias electric field (a) $E_{bias} = 0$ and (b) $E_{bias} = 2 \text{ kV mm}^{-1}$ (b). The applied stress is $\sigma = -50 \text{ MPa}$. The corresponding polarization responses of the sample are shown in graph (c) and (d).

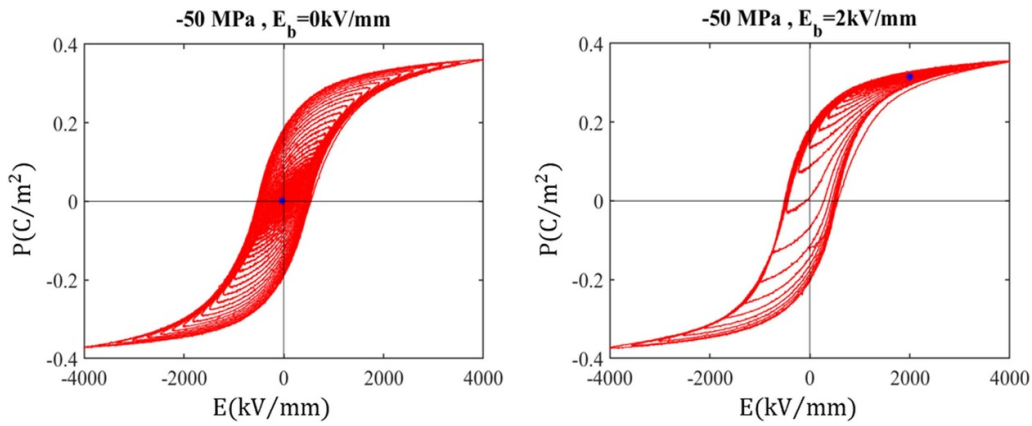


Figure 3. The graph shows the results for a compressive stress of 50 MPa, of the second and third steps, in red the $P(E)$ loops corresponding to the cyclic depoling of the NCE55, the blue point is P_{an} corresponding to the E_{bias} defined.

surface. Assuming homogeneity in the sample, averaging is performed over the surface to derive a single value corresponding to each level of the electric field. Figure 4 shows the $S(E)$ signal obtained during steps three and four of figure 2(a). It is not easily possible to obtain a common reference between stress levels. Therefore, each anhyseretic strain curve is plotted with its independent strain reference value. The reference values are arbitrarily chosen to be the state at the maximum electric field: for each curve, images are correlated with the image obtained at the maximum electric field (yellow point on figure 4). The ten anhyseretic strains obtained during step three are averaged to increase the measurement precision. The resulting anhyseretic point is highlighted by a red circle.

3. Results and discussion

Figure 5 shows in red the $P(E)$ signal obtained from figures 2(a) and (c) (measurement of the anhyseretic point at $E_{bias} = 0$). It also shows in blue the complete anhyseretic $P-E$ curve obtained under -3 MPa and -50 MPa after collecting all anhyseretic points. The anhyseretic curve fits

within the hysteretic loop. It passes through the origin and reaches saturation at high fields. Hysteretic and anhyseretic values are close at a high electric field since the saturation state is equivalent in both cases. The anhyseretic polarization curve (blue curve) at a low electric field is more abrupt than the hysteretic polarization curve (red curve) at the coercive field. It is believed that the motion of domain walls is impeded by pinning effects during the entire hysteretic loop, coercive fields included. The susceptibility at the polarization reversals is consequently reduced.

Figure 6 shows the anhyseretic $S-E$ curve superimposed on the classical $S-E$ major loop. Figure 6(a) shows the longitudinal strain component and figure 6(b) the transverse one. The $S-E$ major loop is measured under a 1 mHz sine electric field. The zero-strain reference is defined to be the anhyseretic strain for $E_{bias} = 0$ (i.e. the depolarized material state). Similarly, to the anhyseretic polarization curve, the anhyseretic strain curve fits within the $S-E$ area. For a better understanding of the differences between a hysteretic and an anhyseretic state, the microstructural state of the material is schematically illustrated at the grain scale for the three states

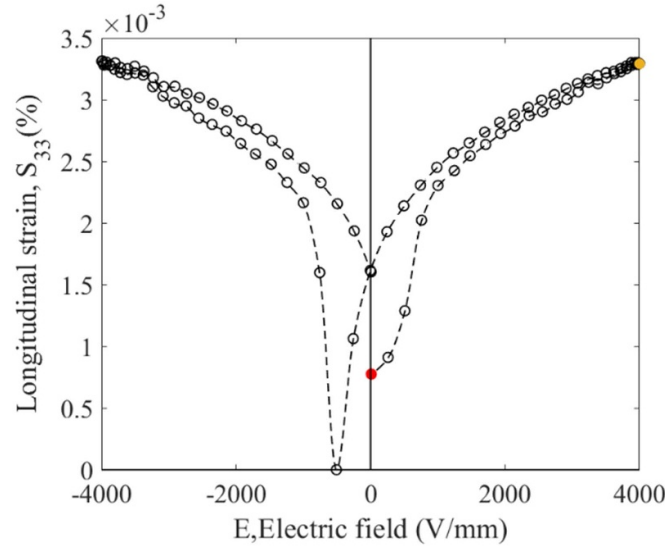


Figure 4. $S(E)$ signal obtained from the 110 captured images of the two final steps. The applied $E(t)$ is the signal in figure 2(a) ($E_{\text{bias}} = 0$). The reference point is illustrated by a yellow point.

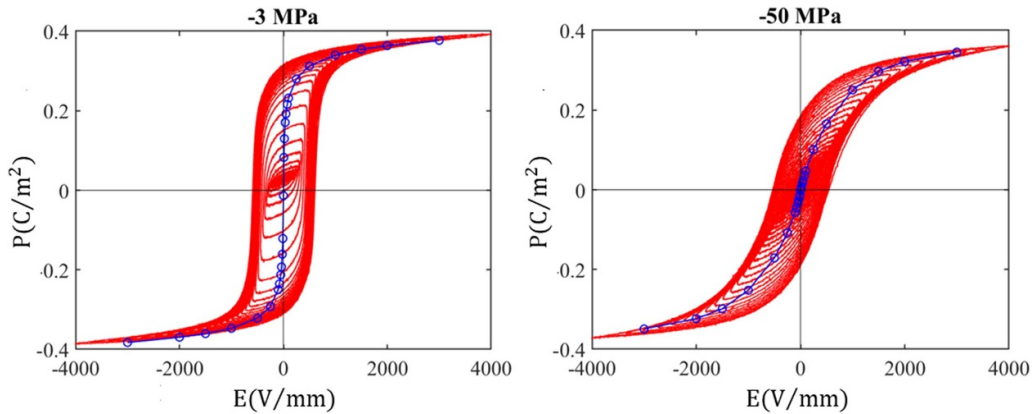


Figure 5. $P(E)$ anhyseretic response of NCE55 for a compressive stress of 3 MPa (left) 50 MPa (right) obtained following the protocol designed in figure 2.

(figure 6(c)). The dashed lines represent the domain walls and arrows show the domain direction.

State (1) corresponds to the minimal strain value of the S - E hysteretic loop (near coercive field). At this point, the polarization is switching from a positive value to a negative value. The local polarization distribution is anisotropic. The volume fraction of 90° oriented domains is maximum, as illustrated. The longitudinal strain is then even lower than the longitudinal anhyseretic strain at $E = 0$.

State (2) corresponds to the anhyseretic point at zero electric field. Similarly to state (1), the material is macroscopically unpoled ($P = 0$). However, the domain distribution is quite different. In state (2), domains are randomly oriented, as opposed to state (1) where domains are mainly aligned perpendicular to the electric field direction. The macroscopic ferroelastic strain is thus null in state (2), contrary to state (1) which exhibits a negative strain.

In state (3), the longitudinal ferroelastic strain is maximum. The polarization of domains is preferentially oriented in the direction of the electric field. This microstructural state is the

same whatever the electric field history. In other words, both the hysteretic and anhyseretic behavior led to this state over the saturating electric field.

The longitudinal S - E loop amplitude is 3.75×10^{-3} and the transverse S - E loop amplitude is 1.75×10^{-3} . The corresponding anhyseretic strain amplitudes is 2.55×10^{-3} (longitudinal strain) and 1.25×10^{-3} (transverse strain). The ratios between transverse and longitudinal strain components are similar for the hysteretic S - E curves (47%) and for the anhyseretic curves (49%). Assuming that the transverse strain S_{22} is equal to S_{11} (transverse isotropic behavior), this suggests a negligible volume change of the sample during poling.

Anhyseretic strain measurements are performed over a series of levels of unidirectional compressive stresses (parallel to the electric field) to understand how ferroelectrics behave under different stimuli and identify the reversible and irreversible behavior (figure 7).

Using strain at saturation as a reference would be optimal, as this saturation microstructure is identical regardless of the sample loading history. However, achieving saturation

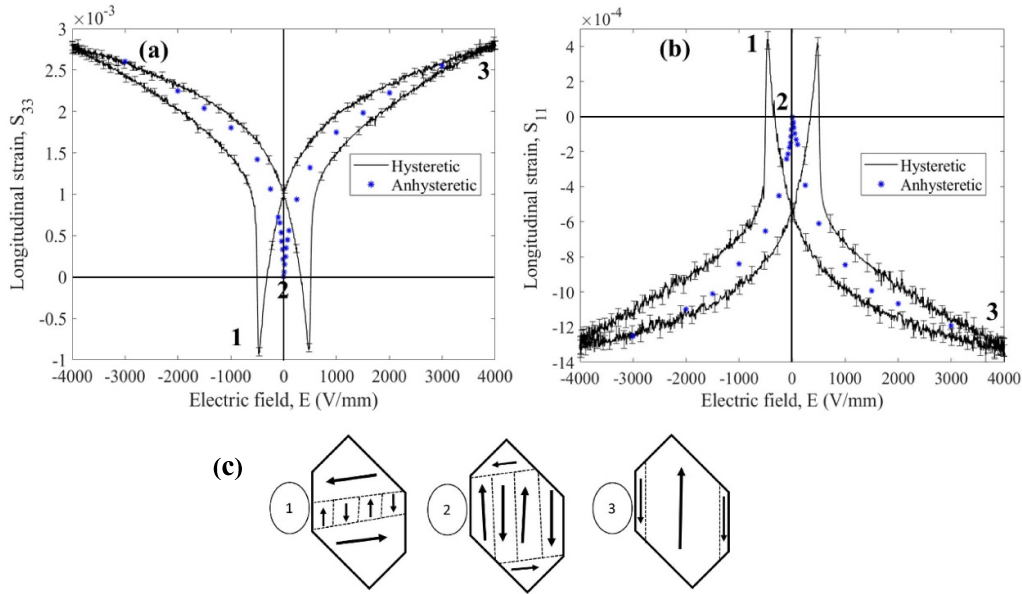


Figure 6. Longitudinal S - E butterfly loop (black solid line) and longitudinal anhyseretic strain curve (blue dots) (a); transverse S - E butterfly loop (black solid line) and transverse anhyseretic curve (blue dots) (b) obtained for a NCE55, Noliac; Alteration of the polarization of domains within a grain in response to the applied electric field (c). The major loops are obtained with a sine electric field of 1 mHz. Their error bars, in black, are about $\pm 5 \times 10^{-5}$.

demands a higher electric field, which poses a risk of breaking the samples. Consequently, aligning the strain curves corresponding to each stress level with the saturation point is not feasible. Instead, they are positioned arbitrarily (figure 7).

Figure 8 shows the evolution of the apparent piezoelectric coefficients d_{33}^* and d_{31}^* as a function of the electric field for different levels of compressive loading. The piezoelectric coefficients are calculated from anhyseretic strains curves, with $d_{33}^* = \frac{S_{33}}{E}$ and $d_{31}^* = \frac{S_{11}}{E}$.

The measurements indicate a monotonous evolution of d_{33}^* and d_{31}^* with stress. The anhyseretic piezoelectric coefficient d_{33}^* decreases with increasing magnitudes of compressive stress. Initially, the rate of decrease is significant from 0 to -25 MPa, but then it starts to reduce. Around -100 MPa, the decrease in d_{33}^* tends to reach saturation. Conversely, d_{31}^* is observed to increase with increasing stress. The rate of increase is notable from 0 to -25 MPa, but it starts to slow down from -25 to -100 MPa, also showing a tendency to reach saturation around -100 MPa. The evolution of the anhyseretic piezoelectric coefficients is monotonous compared to the evolution of the hysteretic piezoelectric coefficients as shown in [38], where d_{33}^* and d_{31}^* exhibit a peak between -25 and -100 MPa for low electric field. The stress level corresponding to the peak increases as a function of the applied electric field.

The study also examined the correlation between polarisation and strain, with measurements indicating a hysteretic dependence of strain on polarisation (see figure 9). In particular, hysteresis decreases with increasing compressive stress amplitude. It is also observed that at higher stress levels, the anhyseretic curve tends to correspond closely to the skeleton of the S - P butterfly curve.

Compressive stress decreases very significantly the dielectric permittivity. Because the tests are performed at fixed maximum electric field, the polarisation reached decreases with the applied compressive stress. As a result, less domain switching is involved, reducing the overall hysteresis area. If the tests were performed at fixed maximum polarisation, the opposite would be found, with an increase of the loop area with the applied compressive stress. The compressive stress modifies the piezoelectric properties as shown in the results section. These effects are explained as well in [40].

Figure 10(a) shows an example of hysteretic and anhyseretic strain measurement (under no applied stress) and figure 10(b) shows the evolution of the magnitude of strains as a function of the applied compressive stress. It can be noticed that the amplitude of strain (both hysteretic and anhyseretic) first increases with stress and then decreases. Indeed, the theoretical saturation state is a configuration for which domains are oriented close to the poling direction. The maximum strain amplitude is then obtained if the initial configuration (under no applied electric field) contains a maximum of orientations perpendicular to the poling direction. Poling will then induce more 90-domain switching, hence higher strains. Because compressive stress facilitates the existence of domains perpendicular to the stress direction, the strain amplitude logically increases with stress. At higher stress levels, the applied electrical fields is not high enough to saturate the material, hence the decrease of the strain amplitude. In other words, stress contributes to decrease both the initial and final strain levels, but at different rates. It can also be noticed that, as compressive stress increases, the difference between the magnitude of anhyseretic and hysteretic strains decreases. This

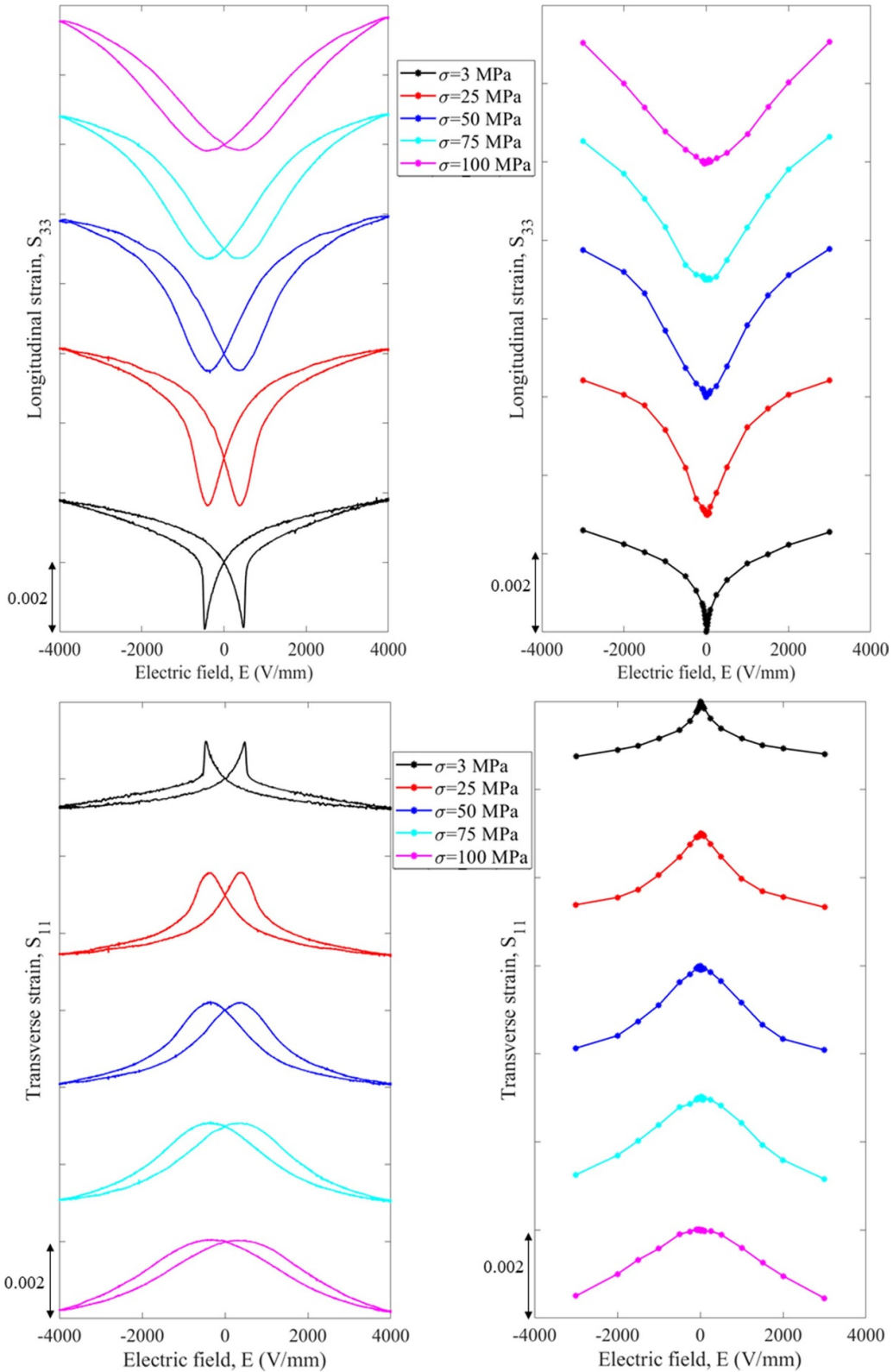


Figure 7. Anhysteretic (connected dots) and hysteretic (line) strain-electric field curves of NCE55 for different levels of compressive stress.

can be explained by the fact that at high stress, stress dominates the definition of both initial and high-field domain configurations. As a consequence, the strain amplitude, defined by

the contrast between these two domain configurations, is the same independently of the electric field path, hysteretic or anhysteretic.

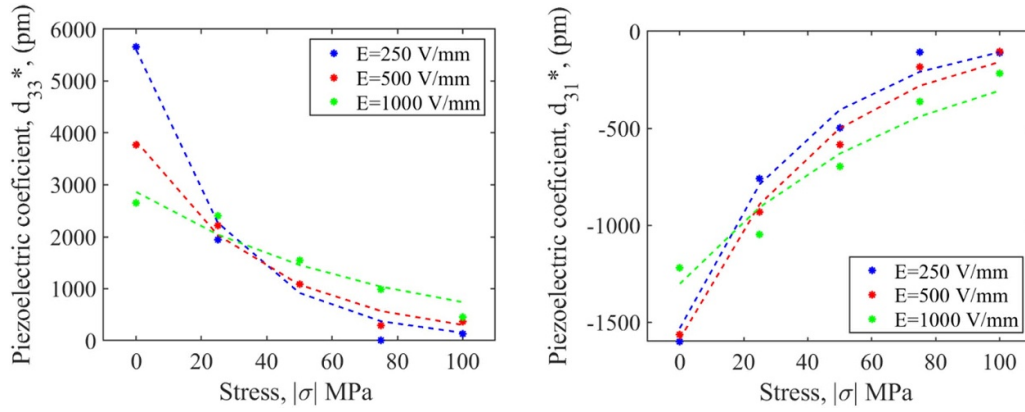


Figure 8. Evolution of the apparent anhysteretic piezoelectric coefficients under compressive loading. The dashed lines are a guide for the eyes.

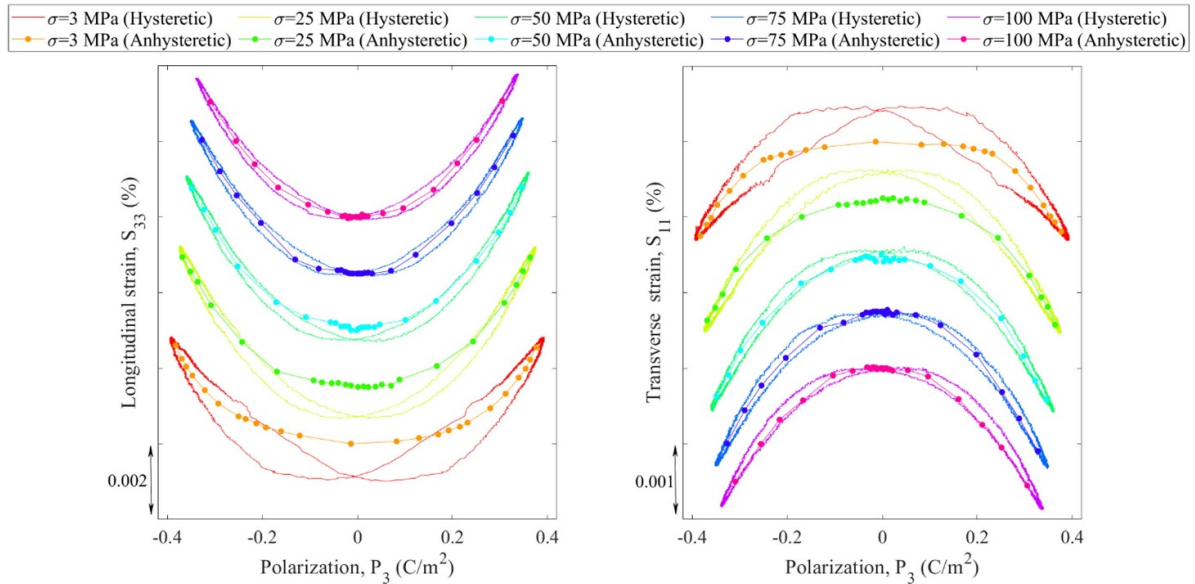


Figure 9. Longitudinal and transverse strain-polarisation curves of NCE55 for different compressive stress levels. The connected dots represent the anhysteretic Strain-polarisation curve.

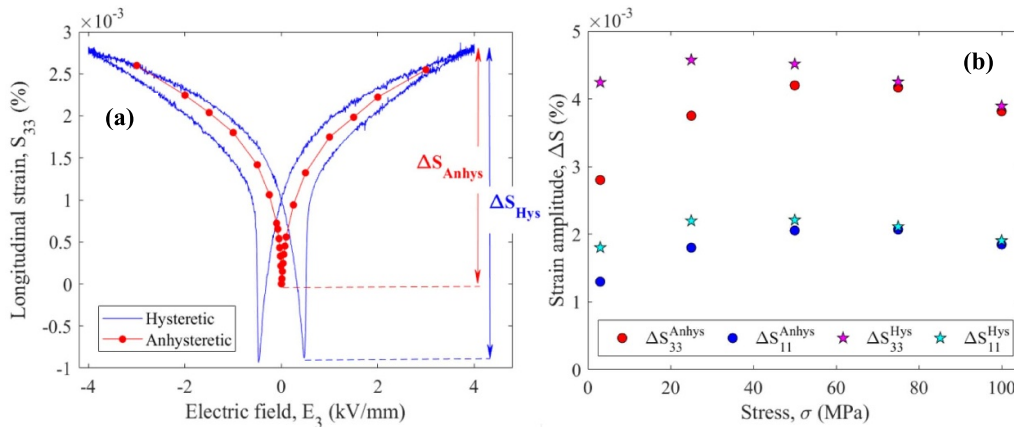


Figure 10. Ferroelectric strain: (a) Strain butterfly loop and anhysteretic ferroelectric strain curves under no applied stress. (b) The magnitude of anhysteretic and hysteretic strains as a function of the applied compressive stress.

4. Conclusion

In this study, a protocol is proposed for measuring the anhysteretic longitudinal strain and transverse strain of PZT by DIC method. This concept of anhysteretic strain should help theoretical studies of ferroelectric behavior by separating the reversible and dissipative contributions to the macroscopic behavior. These anhysteretic measurements eliminate the influence of defects and dissipation on material behavior. The anhysteretic strain appears to be isochoric (the ratio between transverse and longitudinal strain is very close to 50%). Anhysteretic curves allow to differentiate between the stable configuration of the domain structure and additional factors leading to dissipation, such as defects. In this study such an approach was implemented to investigate the effect of compressive stress on both hysteretic and anhysteretic strain responses of a soft PZT.

The developed procedure contributes to the fundamental understanding of ferroelectric behavior and holds promise as a practical tool for advancing the design of synthetic ferroelectric materials. The anhysteretic curve can be a major asset in modelling ferroelectric behavior. The ability to distinguish and analyze reversible and irreversible behavior independently improves the ability to develop accurate models with a physical basis, contributing to the overall understanding of material behavior.

Data availability statement

All data that support the findings of this study are included within the article (and any supplementary files).

ORCID iDs

Chaimae Babori  <https://orcid.org/0000-0003-3742-0677>

Laurent Daniel  <https://orcid.org/0000-0001-5016-4589>

References

- [1] Borgmann H 2016 *15th Int. Conf. on New Actuators & 9th Int. Exhibition on Smart Actuators and Drive Systems* (available at: <https://books.google.fr/books?id=S293AQAACAAJ>)
- [2] Mahbub I, Pullano S A, Wang H, Islam S K, Fiorillo A S, To G and Mahfouz M R 2017 A low-power wireless piezoelectric sensor-based respiration monitoring system realized in CMOS process *IEEE Sens. J.* **17** 1858–64
- [3] Carioli J, Delnavaz A, Zednik R J and Voix J 2018 Piezoelectric earcanal bending sensor *IEEE Sens. J.* **18** 2060–7
- [4] Dagdeviren C et al 2014 Conformal piezoelectric energy harvesting and storage from motions of the heart, lung, and diaphragm *Proc. Natl Acad. Sci. USA* **111** 1927–32
- [5] Kwok K F, Dong P, Cheng K W E, Kwok K W, Ho Y L, Wang X X and Chan H 2004 General study on piezoelectric transformer *Proc. 2004 First Int. Conf. Power Electron. Syst. Appl. 2004* pp 216–20
- [6] Lynch C S 1996 The effect of uniaxial stress on the electro-mechanical response of 8/65/35 PLZT *Acta Mater.* **44** 4137–48
- [7] Stewart M, Cain M and Hall D 1999 *Natl Phys. Lab. Rep. C* **152** P1–P5
- [8] Glazer A M, Groves P and Smith D T 1984 Automatic sampling circuit for ferroelectric hysteresis loops *J. Phys. E: Sci. Instrum.* **17** 95–97
- [9] Hall D A 2001 Nonlinearity in piezoelectric ceramics *J. Mater. Sci.* **36** 4575–601
- [10] Wang D and Mottershead J E 2016 Measurement precision and spatial resolution with Kriging digital image correlation *Stroj. Vestn. J. Mech. Eng.* **62** 419–29
- [11] Stewart M, Battrick W and Cain M G 2001 Measuring piezoelectric d33 coefficients using the direct method *Measurement Good Practice Guide No. 44* (National Physical Laboratory)
- [12] Fialka J and Benes P 2013 Comparison of methods for the measurement of piezoelectric coefficients *IEEE Trans. Instrum. Meas.* **62** 1047–57
- [13] Torón B, Szperlich P, Nowak M and Starczewska A 2023 A novel method for measuring piezoelectric coefficients *Measurement* **206** 112274
- [14] Bar-Chaim N, Brunstein M, Grünberg J and Seidman A 1974 Electric field dependence of the dielectric constant of PZT ferroelectric ceramics *J. Appl. Phys.* **45** 2398–405
- [15] Wang Z, Khandelwal S and Khan A I 2017 Ferroelectric oscillators and their coupled networks *IEEE Electron Device Lett.* **38** 1614–7
- [16] Ishiwara H 2012 Ferroelectric random access memories *J. Nanosci. Nanotechnol.* **12** 7619–27
- [17] Panda P K, Sahoo B and Thejas T S 2023 High strain lead-free piezo ceramics for sensor and actuator applications: a review *Sensors Int.* **4** 100226
- [18] Zhou D, Wang R and Kamlah M 2010 Determination of reversible and irreversible contributions to the polarization and strain response of soft PZT using the partial unloading method *J. Eur. Ceram. Soc.* **30** 2603–15
- [19] Maier J G, Gademawla A, Khansur N H and Webber K G 2023 Stress-induced tailoring of energy storage properties in lead-free $\text{Ba}_{0.85}\text{Ca}_{0.15}\text{Zr}_{0.1}\text{Ti}_{0.9}\text{O}_3$ ferroelectric bulk ceramics *J. Mater.* **9** 673–82
- [20] Kaeswurm B, Segouin V, Daniel L and Webber K G 2018 The anhysteretic polarisation of ferroelectrics *J. Phys. D: Appl. Phys.* **51** 075305
- [21] Daniel L, Hall D A and Withers P J 2014 A multiscale model for reversible ferroelectric behaviour of polycrystalline ceramics *Mech. Mater.* **71** 85–100
- [22] Babori C, Barati M and Daniel L 2024 An energy-based model for ferroelectric ceramics *Eur. J. Mech. A* **103** 105151
- [23] Bozorth R M 1951 *Ferromagnetism* (Van Nostrand Company)
- [24] Jiles D 1991 *Introduction to Magnetism and Magnetic Materials* (Chapman and Hall) (<https://doi.org/10.1007/978-1-4615-3868-4>)
- [25] Cullity B D and Graham C D 2011 *Introduction to Magnetic Materials* (Wiley)
- [26] Daniel L and Domenjoud M 2021 Anhysteretic magneto-elastic behaviour of terfenol-d: experiments, multiscale modelling and analytical formulas *Materials* **14** 5165
- [27] Segouin V, Kaeswurm B, Webber K G and Daniel L 2018 Temperature-dependent anhysteretic behavior of co-doped PZT *J. Appl. Phys.* **124** 104103
- [28] Webber K G n.d. Ceramic and single-crystal (1-x)PMN-xPT constitutive behavior under combined stress and electric field loading *Acta Mater.* **56** 1219–27
- [29] Zaman A, Iqbal Y, Hussain A, Kim M H and Malik R A 2014 Dielectric, ferroelectric, and field-induced strain properties of ta-doped $0.99\text{Bi}_{0.5}(\text{Na}_{0.82}\text{K}_{0.18})_{0.5}\text{TiO}_{3-0.01}\text{LiSbO}_3$ ceramics *J. Mater. Sci.* **49** 3205–14
- [30] Sutton M A, Orteu J J and Schreier H 2009 *Image Correlation for Shape, Motion and Deformation Measurements: Basic Concepts, Theory and Applications* (Springer Science & Business Media)

- [31] Sánchez-Arévalo F M, García-Fernández T, Pulos G and Villagrán-Muniz M 2009 Use of digital speckle pattern correlation for strain measurements in a CuAlBe shape memory alloy *Mater. Charact.* **60** 775–82
- [32] Ozbulut O E, Daghash S and Sherif M M 2015 Shape memory alloy cables for structural applications *J. Mater. Civ. Eng.* **28** 04015176
- [33] Pan B, Wu D, Wang Z and Xia Y 2010 High-temperature digital image correlation method for full-field deformation measurement at 1200 °C *Meas. Sci. Technol.* **22** 015701
- [34] Zighem F, Belmeguenai M, Faurie D, Haddadi H and Moulin J 2014 Combining ferromagnetic resonator and digital image correlation to study the strain induced resonance tunability in magnetoelectric heterostructures *Rev. Sci. Instrum.* **85** 103905
- [35] Segouin V, Domenjoud M, Bernard Y and Daniel L 2019 Mechanics-aided digital image correlation for the investigation of piezoelectric and ferroelectric behaviour of a soft PZT *J. Eur. Ceram. Soc.* **39** 2091–102
- [36] Malakooti M H and Sodano H A 2013 Direct measurement of piezoelectric shear coefficient *J. Appl. Phys.* **113** 214106
- [37] Chen D and Kamlah M 2015 Deformation in lead zirconate titanate ceramics under large signal electric field loading measured by digital image correlation *Rev. Sci. Instrum.* **86** 113707
- [38] Segouin V, Domenjoud M, Bernard Y and Daniel L 2021 Electro-mechanical behaviour of ferroelectrics: insights into local contributions from macroscopic measurements *Acta Mater.* **211** 116870
- [39] Tomičević Z, Hild F and Roux S 2013 Mechanics-aided digital image correlation *J. Strain Anal. Eng. Des.* **48** 330–43
- [40] Zhou D, Kamlah M and Munz D 2005 Effects of uniaxial prestress on the ferroelectric hysteretic response of soft PZT *J. Eur. Ceram. Soc.* **25** 425–32